Title

Acquisition of chemical remanent magnetization during experimental ferrihydrite–hematite conversion in Earth-like magnetic field—implications for paleomagnetic studies of red beds

Authors

Jiang, Zhaoxia
Liu, Qingsong
Dekkers, Mark J
et al.

Publication Date

2015-10-01

DOI

10.1016/j.epsl.2015.07.024

Peer reviewed

Acquisition of chemical remanent magnetization during experimental ferrihydrite-hematite conversion in Earth-like magnetic field—implications for paleomagnetic studies of red beds

Zhaoxia Jiang[a], Qingsong Liu*[a], Mark J. Dekkers[b], Lisa Tauxe[c], Huafeng Qin[a], Vidal Barrón[d], José Torrent[d]

[a] State Key Laboratory of Lithospheric Evolution, Institute of Geology and Geophysics, Chinese Academy of Sciences, Beijing 100029, China

[b]Department of Earth Sciences, Paleomagnetic Laboratory 'Fort Hoofddijk', Faculty of Geosciences, Utrecht University, Budapestlaan 17, 3584 CD Utrecht, The Netherlands

[c]Scripps Institution of Oceanography, University of California San Diego, San Diego, CA 92093-0220, USA

[d]Departamento de Agronomía, Universidad de Córdoba, Edificio C4, Campus de Rabanales, 14071 Córdoba, Spain

*Corresponding author: Qingsong Liu (qsliu@mail.iggcas.ac.cn;Tel:+861082998365)

Abstract

Hematite-bearing red beds are renowned for their chemical remanent magnetization (CRM). If the CRM was acquired substantially later than the sediment was formed, this severely compromises paleomagnetic records. To improve our interpretation of the natural remanent magnetization, the intricacies of the CRM acquisition process must be understood. Here, we contribute to this issue by synthesizing hematite under controlled 'Earth-like' field conditions (< ~100 μT). CRM was imparted in 90 oriented samples with varying inclinations. The final magnetic remanence carrier is hematite with traces of ferrimagnetic ferrihydrite or maghemite. When the magnetic field intensity is > ~40 μT, CRM of hematite records the field direction faithfully. However, for growth field intensities < ~40 μT, the CRM direction may deviate considerably from that of the growth field. The CRM intensity normalized by the isothermal remanent magnetization ($CRM/IRM_{@2.5\ T}$) increases linearly with the intensity of growth field, implying that CRM could potentially be useful for relative paleointensity studies. The hematite CRM has a distributed unblocking temperature spectrum from ~200 to ~650 °C while hematite with a depositional remanent magnetization (DRM) has a more confined spectrum from ~600 to 680 °C. Further, the CRM thermal demagnetization curves with their concave shape are notably different from their DRM counterparts which are convex. These differences together are suggested to be a potential discriminator of CRM from DRM carried by hematite in natural red beds, and of significance for the interpretation of paleomagnetic studies on red beds.

Key words: Hematite, crystal growth, chemical remanent magnetization (CRM), detrital remanent magnetization (DRM)

1. Introduction

Red beds, the detrital sedimentary rocks pigmented by hematite (Robb, 1949; Walkers, 1967; Van Houten, 1968; Collinson, 1974), are widely distributed in tropical and subtropical areas (Van Houten, 1973; Dunlop and Özdemir, 2001) and have been extensively used for paleomagnetic studies (Tauxe et al., 1980; Kent et al., 1986; Tan et al., 2003; Iosifidi et al., 2010). The detrital hematite is usually the dominant and faithful magnetization carrier in red beds (Collinson, 1966, 1974; Tauxe et al., 1980). However, paleomagnetic records of red beds are often affected by chemical remanent magnetization (CRM) acquired after deposition residing in authigenic hematite (Kent et al., 1987; McCabe and Elmore, 1989; Wang and Van der Voo, 1993; Elmore et al., 2006; Van der Voo and Torsvik, 2012). CRM usually overprints the primary remanent magnetization of red beds – a detrital remanent magnetization (DRM) either partially or completely, and thus complicates paleomagnetic interpretations (Stearns and Van der Voo, 1987; Huang and Opdyke, 1996; Deng et al., 2007; Dekkers, 2012). Therefore, a central aspect of paleomagnetic studies on red beds is to discriminate CRM from DRM in order to discern the primary natural remanent magnetization (NRM) component if possible (e.g. Collinson, 1965; Kodama and Dekkers, 2004; Iosifidi et al., 2010; Liu et al., 2011). To better appreciate the potential range of CRM behavior, the CRM acquisition process should be understood.

CRM is acquired during chemical change of minerals below their Curie or Néel temperatures in the presence of an ambient magnetic field. This occurs during weathering, diagenesis, or metamorphism. CRM formation can be the result of simple crystal growth (growth-CRM) or of the alteration of parent magnetic minerals (alteration-CRM) (e.g. Haigh, 1958; Stokking and Tauxe,1990a; Dunlop and Özdemir, 2001). However, the acquisition of a stable CRM requires magnetic minerals of a

certain minimal size larger than the superparamagnetic (SP) threshold size. Beyond this size range, changes in the external field direction and/or intensity have little or no effect on the remanent magnetization (O'Reilly, 1984; Dunlop and Özdemir, 2001).

To further our understanding of CRM in red beds, the acquisition process of CRM in hematite has been simulated experimentally in the laboratory (Hedley, 1968; Bailey and Hale, 1981; Stokking and Tauxe, 1987,1990a, 1990b; Özdemir and Dunlop, 1993; Gendler et al., 2005). Two types of CRM are distinguished growth-CRM and alteration-CRM: the first involves growing of the magnetic minerals through the SP threshold; the second implies the alteration of an existing magnetic mineral to another magnetic mineral at a temperature below the magnetic ordering temperature. Aspects of alteration-CRM were explored by Marshall and Cox (1971) who investigated the CRM of submarine basalt acquired through mineral transformation (titanomagnetite → titanohematite) during heating in an ambient field. They found that the direction of NRM was not affected by CRM acquisition if the oxidation occurs below the original Curie temperature of the titanomagnetite. However, Bailey and Hale (1981) determined that the CRM direction acquired by submarine basalts during heating in the lab-field of 50 μT is between the ambient field direction and that of the pre-existing NRM. Özdemir and Dunlop (1993) studied the CRM accompanying the phase transformations lepidocrocite → maghemite → hematite in a field of 50 μT from 200 to 650^{o}C. They observed two CRM intensity peaks around 275^{o}C and 400^{o}C which were also detected by subsequent studies of Gendler et al. (2005), where transformations lepidocrocite → maghemite and maghemite → hematite occur respectively, and CRM directions are always at a large angle to the applied field.

For the understanding of growth-CRM the pathway of hematite formation is

important. Hematite can crystallize through various pathways, directly from the hydrolysis of ferric iron salts (Schwertmann and Cornell, 2000) or in more complicated schemes such as the ferrihydrite → ferromagnetic ferrihydrite → hydromaghemite → hematite reaction chain (Barrón and Torrent, 2002; Barrón et al., 2003; Michel et al., 2010). To understand the properties of growth-CRM, Stokking and Tauxe (1987) synthesized hematite crystals in an aqueous ferric nitrate solution in magnetic fields controlled with three orthogonal sets of Helmholtz coils. They found that the CRM was acquired parallel to the applied field. In addition, its intensity was a linear function of the field up to 7.5 mT (Stokking and Tauxe, 1990a). However, when two perpendicular fields were applied during hematite growth in two different stages, the CRM behavior became complex (Stokking and Tauxe, 1990b). The resulting CRM could be parallel or antiparallel to, as well as intermediate between these two fields (Stokking and Tauxe, 1990b), underscoring the complexity inherent to the process of remanence acquisition by crystals precipitating from solution. Therefore, how to interpret CRM directions in terms of ancient field directions is not straightforward.

Previous studies investigated either processes at certain single field values or a large range of typically rather strong growth fields (~0-7.5 mT). No study has yet systematically investigated the properties of CRM acquired in fields similar to the earth's magnetic field, which is more relevant for paleomagnetic studies of natural samples. In addition, the relationship of CRM intensity versus applied field has not been investigated systematically, apart from the study by Stokking and Tauxe (1990a) who discussed the variation of CRM intensity through a range of fields (~0-7.5 mT).

To study the behavior of CRM versus applied field under earth-like field

conditions, we synthesized a series of hematite samples in 2×2×2 cm^3 cubes. Ferrihydrite was transformed to hematite under controlled conditions (fields: ~10 – 100 μT, temperature: 95 ^oC). The CRM and other magnetic properties of these samples grown under different field strengths are reported here, and their paleomagnetic significance for red bed studies will also be discussed.

2. Sample preparation and methods

2.1. Sample preparation

Ferrihydrite was synthesized by mixing 100 mL 0.5 M Fe $(NO_3)_3$ and 100 mL of 2 M NaOH. Subsequently 50 mL 1 M $NaHCO_3$ was added to bring the pH to ~7. The deionized water for the solutions was heated to 90 ^oC in advance to inhibit the formation of goethite. The resulting brown ferrihydrite suspensions (the precursor of hematite) were centrifuged and the supernatant solution was preserved in a cylinder to age the hematite. To prevent DRM acquisition, the fresh ferrihydrite was mixed with quartz wool and then pressed fully into ceramic boxes (2×2×2 cm^3). The quartz wool and ceramic boxes were thermally demagnetized to 700 °C before being used in order to remove any remanence. Then the cubic ceramic samples were given an orientation line to be able to retain the orientation throughout subsequent sample manipulations. They were mounted in the cylinder containing the supernatant. The ferrihydrite was aged under controlled temperature and field conditions. The temperature of the solution was maintained at 95 ± 3 °C by a small furnace equipped with a digital thermometer. A controlled magnetic field was obtained with two sets of cubic Helmholtz coils (1×1 m^2) which were aligned with the declination of the ambient field in the laboratory. One pair of coils was set horizontal to produce the vertical field component, while the other pair was put vertical to produce the horizontal component.

In this manner CRMs with nearly zero declination and with any desired inclination can be imparted. The iron oxides were grown in nine different magnetic field strengths; the directions and strengths are summarized in Table 1. For each field setting, twelve samples were obtained. The sample series are labeled CRM1* (100.8 μT), CRM2* (85.7 μT), CRM3* (67.6 μT), CRM4* (54.7 μT), CRM5* (44.2 μT), CRM6* (37.9 μT), CRM7* (24.2 μT), CRM8* (16.2 μT), and CRM9* (11.9 μT). The aging was almost completed in two weeks as confirmed by a trial experiment with susceptibility measurement made every day. Thereafter the samples were dried and cooled in a field-free space to avoid the acquisition of a partial thermal remanent magnetization (pTRM). The dried samples were kept in a magnetically shielded room with residual field < 300 nT prior to making the magnetic measurements.

2.2. Experimental methods

The anisotropy of magnetic susceptibility (AMS) of these samples was first measured using an AGICO KLY-4S Kappabridge. The remanent magnetizations were measured with a cryogenic magnetometer system (2G Enterprises 760R) installed in the magnetically shielded room with residual field < 300 nT. Firstly, all the samples were subjected to progressive alternating field (AF) demagnetization to resolve a possible soft remanence component in the samples, i.e., potential contamination of maghemite or ferromagnetic ferrihydrite. Then each sample series was divided into two groups; one group of samples was used to measure the isothermal remanent magnetization acquired at 2.5 T field ($IRM_{@2.5\ T}$), and the other group of samples was subjected to stepwise thermal demagnetization from 80 °C to a maximum temperature of 700 °C with 10 °C intervals between 80 and 150 °C and between 600 and 700 °C to precisely resolve potential goethite and hematite remanences respectively. Between 150 and 600 °C the demagnetization interval was 50 °C. A Magnetic Measurements

thermal demagnetizer with a residual magnetic field < 10 nT was used for this purpose.

The group of samples that were subjected to the $IRM_{@2.5\ T}$ measurement were removed from the ceramic boxes afterwards for rock magnetic measurements. Samples were ground to powder and then filtered with 200 meshes sieve to remove the quartz wool. Firstly, IRM acquisition curves with 80 steps were measured with a maximum field 2 T on a Princeton Measurements Corporation vibrating sample magnetometer (Micromag VSM 3900) at room temperature. The IRM acquisition curves were decomposed into magnetic coercivity components using the method of Kruiver et al. (2001) that works with the premise that the measured IRM acquisition curves can be represented by a linear addition of coercivity components represented by cumulative log-Gaussian functions. Subsequently, the back-field curves were measured to determine remanent coercivity (B_{cr}). Hysteresis loops for all these samples were measured at room temperature in 5 mT increments using a Micromag VSM 3900 with a maximum field of 2 T. Finally, the thermomagnetic curve in a steady field of 1 T (J-T) curve was measured from room temperature to 800°C, using a Magnetic Measurements Variable Field Translation Balance (VFTB) in air.

3. Results

3.1. Characterization of growth material

X-ray diffractograms (XRD) of the powder samples (Figure 1) show that hematite can be detected, while the dominant mineral observed is sodium nitrate ($NaNO_3$) which is the main component of the supernatant solution (containing Na^+, NO_3^- and HCO_3^-). The HCO_3^- equilibrates with the atmosphere and is removed as CO_2, so only $NaNO_3$ is formed.

As shown by the J-T curves of selective samples (Figure 2 a1, b1, c1, d1), no

clear Néel temperature of hematite can be observed and the J-T curves display hyperbolic type, which is due to the dominant effects of superparamagnetic (SP) minerals. The cooling branches are lower than the corresponding heating branches for all samples which may result from crystal healing of these samples. Hysteresis loops and the acquisition curves of IRM show that these samples are far from saturated even in a 2 T field, so B_{cr} acquired from back field curves is a minimum estimate. Hysteresis loops exhibit a ramp-like shape, demonstrating the presence of SP particles. In addition, The IRM component analyses indicate the presence of two magnetic components, a relatively low coercivity (L) component with a mean coercivity ($B_{1/2L}$) ranging between 22~40 mT, and a high coercivity (H) component with a mean coercivity ($B_{1/2H}$) larger than 1 T (Figure 2 a4, b4, c4, d4, Table 2). Apparently, the IRM of these samples is dominated by the high coercivity component which contributes 85 ~ 98% of the IRM (Table 2). B_{cr} decreases with decreasing growth field except CRM6* series (37.9 μT), which is consistent with the variation trend of $B_{1/2H}$.

3.2. CRM characterization

The AMS results of these oriented samples are barely above the instrument noise level. The representative four series of samples have very low anisotropy degrees (P) with the majority being < 1.01 without a tendency for oblate or prolate shapes (Figure 3). Each component of magnetic susceptibility is distributed randomly in equal area projection, so the growth field does not impact the orientation of the AMS tensor.

AF demagnetization up to 100 mT of these samples typically removes only ~10% of the CRM, and at most ~20% (Figure 4), indicating that they are magnetically hard and only slightly contaminated (if at all) with ferromagnetic phases, which are an intermediate product in the transformation of ferrihydrite to hematite (Michel et al., 2010). After AF demagnetization, the samples were subjected to progressive stepwise

thermal demagnetization: the CRM decays univectorially to the origin (Figure 5). The ChRM can be isolated between 200 and 640°C, demonstrating that pigmentary hematite is the major magnetic carrier. An inflection can be detected around 300°C which may be the signal of the intermediate ferromagnetic ferrihydrite transforming to hematite around 300 °C. The wide range of blocking temperatures can be attributed to a varying particle size distribution. The remanence residing in the synthetic hematite, after thermal demagnetization to 200°C, is indeed a CRM.

The directions of the initial CRM, ChRM, and their growth fields are plotted on equal area stereographic projection in Figure 6. After the initial CRM measurements, each series of samples was divided into two groups, so the number of ChRM data points is less than that of the initial CRM directional data. Results show that for samples grown in fields > ~40 μT, the field direction, CRM and ChRM directions are almost overlapping, that is, CRM records the applied field direction faithfully. For samples grown in fields < ~40 μT, however, the CRM direction significantly deviates from that of applied field, especially for samples grown in fields < ~20 μT with deviations in direction larger than ~40^{o} (Figure 6 and Table 1).

The intensity of CRM versus the growth field plot in the range of 0 to ~100 μT (Figure 7a) is rather scattered, showing only a broad intensity increase with the applied field. The CRM intensity of our samples ranges from 1 to 16×10^{-8} Am^{2}, but the CRM intensities for samples growing in the same field are quite dispersed, especially for samples produced in a field of 100.8 μT which show intensity deviations up to 25%. Since it is difficult to quantify the hematite concentration in each sample, the CRM was normalized by $IRM_{@2.5\ T}$ for each individual sample to exclude the influence of mass difference (Figure 7b). CRM intensity appears to be 2-12‰ of that of $IRM_{@2.5\ T}$. The value of $CRM/IRM_{@2.5\ T}$ increases linearly with the

growth field, which is consistent with the results of Stokking and Tauxe (1990a).

4. Discussion

4.1. Characterization of final material

For the hematite reaction route of ferrihydrite → ferromagnetic ferrihydrite → maghemite → hematite, the final material will depend on the aging time (Barrón and Torrent, 2002; Michel et al., 2010). If the aging time is not sufficiently long to complete the reaction, the samples are usually composed of SD hematite and intermediate products (ferrimagnetic ferrihydrite or maghemite), both mostly as SP particles (Liu et al., 2008). The ramp-like hysteresis loops of our samples confirm the existence of finer magnetic particles. However, these SP particles cannot contribute to the remanence. The IRM spectrum analysis shows that only two coercivity components can be detected, an "L" component with $B_{1/2L}$ around 22-40 mT and an "H" component with $B_{1/2H}$ around 1-2 T. Since no goethite signal can be observed during the thermal demagnetization process, then the H component is interpreted to be hematite, while the L component may be caused by the fine-grained ferromagnetic maghemite or ferrihydrite, which contributes less than 20% IRM, consistent with the AF demagnetization behavior of the CRM. In addition, as our samples aged in the supernatant solution containing $NaNO_3$ and $NaHCO_3$, the final dry samples should include abundant crystalline $NaNO_3$, a prediction confirmed by the XRD results (Figure 1).

4.2. The dependence of CRM on the applied magnetic field

The relationship between growth CRM and the applied magnetic field is described by the following equations (Stacey and Banerjee, 1974; Stokking and Tauxe, 1990a),

$$M_{CRM} = M_s B \int_0^{\frac{\pi}{2}} \tanh \frac{m_b \cos\theta}{kT} \cos\theta \sin\theta d\theta \qquad (1)$$

$$\frac{M_{CRM}}{M_s} = B \int_0^{\frac{\pi}{2}} \tanh \frac{m_b \cos\theta}{kT} \cos\theta \sin\theta d\theta \qquad (2)$$

Where M_s is the saturation magnetization at the temperature of CRM acquisition, m_b is the grain moment at the blocking volume, B is the magnetic field intensity, and θ is the angle between the applied field and the "easy" direction of the grain. It follows from these equations that growth-CRM should be parallel to the applied magnetic field. The "normalized" CRM intensity, i.e. CRM intensity divided by M_s, is proportional to the applied magnetic field under the proviso M_s and m_b remain constant (Stokking and Tauxe,1990a; McClelland, 1996).

As expected from theory, no inclination shallowing occurs in CRM. Our results show that the CRM directions of hematite closely track the growth field orientation when the magnetic field intensity is higher than ~40 μT (Figure 6), which is consistent with Stokking and Tauxe (1987). However, previous studies show that DRM carried by detrital hematite can suffer from serious inclination shallowing which can complicate the interpretation of paleomagnetic results from red beds (e.g., Tauxe and Kent, 1984; Tan et al., 2007; Bilardello and Kodama, 2010). Hence, CRM recorded shortly after deposition can record the direction of the actual magnetic field and is more suitable for paleomagnetic studies than DRM (Tauxe and Kent, 2004; Mitra and Tauxe, 2009; Iosifidi et al., 2010). However, when the applied field is less than ~40 μT, our synthesis product does not track the applied field in our experiments (Figure 6c-d). It means that CRM formed in low fields may not record the geomagnetic field direction faithfully, such as those insecure remanent acquired during the polarity reversal process owing to the unstable directions and lower intensity of the geomagnetic field (Cox, 1969, 1975; Valet et al., 2005; Leonhardt and

Fabian, 2007). This may be a source of uncertainty in red bed studies that is underappreciated. In this regard, it is interesting to note some 40% of sites performed in magnetostratigraphic studies in red beds, particularly in paleosols, are randomly oriented (e.g., Tauxe and Opdyke, 1982); perhaps this is due to the fact that CRM is unreliable in magnetic fields less than 40 υT and the field is frequently of that magnitude.

Stokking and Tauxe (1990a) synthesized a series of CRM bearing samples and demonstrated that CRM intensity was nearly linearly related to the applied field intensity from 0.015 mT to 7.5 mT (Figure 7c). However, the geomagnetic field intensity is nearly always < 100 μT (e.g. Tauxe et al., 2013). So CRMs acquired in low fields of < 100 μT is more relevant for paleomagnetic studies. Therefore, we compare our results from 10 to 100 μT with those from Stokking and Tauxe (1990a). We normalize the CRM with $IRM_{@2.5\ T}$ for our samples ($CRM/IRM_{@2.5\ T}$) to compare with the CRM data normalized by ARM (CRM/ARM) from Stokking and Tauxe (1990a). The $CRM/IRM_{@2.5\ T}$ or CRM/ARM increases linearly with the applied field from ~0 to 100 μT (Figure 7b), which is in accordance with the theoretical equations.

Although some other magnetic minerals could be present in trace amounts in the final synthesis product, thermal demagnetization curves of the oriented samples demonstrate that hematite is the only magnetic remanence carrier. Therefore, CRM of hematite can record the geomagnetic field intensity faithfully. In other words, CRM recorded by hematite can in principle be used for relative paleointensity studies in the earth-like field range, which is significant for paleomagnetic studies of red beds. However, the prolonged growth of CRM in nature should be considered which may average out the short-lived intensity peaks and troughs.

4.3. Discrimination of CRM and DRM of red beds

Two kinds of hematite, black (specular) grains and red pigment, are known in soils and red beds. Fine-grained chemically formed hematite is responsible for the characteristic color of red beds and is the dominant magnetic carrier in some red beds in warm and humid climates (Robb, 1949; Walker, 1967; Van Houten, 1968; Torrent and Schwertmann, 1987). Detrital hematite, black specularite, is frequently coarser-grained. Tauxe et al. (1980) identified these two kinds of hematites in the Siwalik red beds. The red pigment had a lower and comparatively broad blocking temperature spectrum and higher coercivity, while the black hematite had higher blocking temperatures and lower coercivity. The former can be removed by chemical dissolution and was interpreted to record a chemical remanent magnetization, while the latter most likely carried a detrital remanent magnetization (Tauxe et al., 1980). However, a near primary origin of a CRM can record the direction of the magnetic field faithfully, if the field strength is sufficiently strong. Such remanences are also useful for paleomagnetic reconstruction (Iosifidi et al., 2010). When the prevailing DRM is overprinted by CRM, it is difficult to interpret the resulting magnetization as reflecting the actual information of geomagnetic field (McCabe and Elmore, 1989; Deng et al., 2007). As a result, a reliable means of separating DRM from CRM is indispensable.

McClelland-Brown (1982) successfully used the blocking temperature spectrum to discriminate TRM and CRM in hematite. Inspired by this result, we summarized the stepwise thermal demagnetization curves of our data and previous results (Table 3) in Figure 8, where all the data were normalized by the remanence after demagnetization at 300 °C to remove the influence of viscous remanent magnetization. Our investigations show that the CRM in our samples is completely demagnetized around 600 to 650 °C which is considered to be the maximum unblocking temperature

for our samples (Figure 8b). However, most of the DRM continues to unblock to temperatures up to 660-680 °C (Tauxe et al., 1980; Løvlie et al., 1984; Cogné et al., 1999; Yan et al., 2006; Li et al., 2013), distinctly higher than that of our CRM (Figure 8). Apparently, CRM has a more distributed unblocking temperature spectrum (~200 to 600-650°C) than DRM (mostly 600-680°C). These differences in blocking temperature between CRM and DRM can be attributed to differences in grain size and crystalinity. The DRM of red beds is usually carried by detrital hematite particles with a larger particle size (Collinson, 1965; Steiner, 1983; Tauxe and Kent, 1984), while CRM is carried by newly-formed fine-grained hematite pigment (Collinson, 1966; Tauxe et al., 1980; McClelland-Brown, 1982). Since the blocking temperature is positively related to the particle size of magnetic minerals in the single domain state based on Néel theory (O'Reilly, 1984; Dunlop and Özdemir, 2001), the maximum unblocking temperature of specular hematite (DRM) is higher than that of the pigmentary hematite (CRM). In addition, the decay curves display different shapes. Summarizing the results from previous studies (Tauxe et al., 1980; Løvlie et al., 1984; Tauxe and Kent, 1984; Kent et al., 1987; Stokking and Tauxe, 1987; Cogné et al., 1999; Yan et al., 2006; Liu et al., 2011; Li et al., 2013), DRM demagnetization curves appear to have a convex shapes and drop to zero around 670-680 °C (Figure 8a), but those of CRM display a concave shape and decay to zero gradually (Figure 8b). These distinct differences may be used to distinguish CRM from (most of the) DRM in red beds. Although the unblocking temperature spectrum of DRM recorded in very fine particles will overlap with that of CRM and complicate their distinctions as NRM components, yet our observation is still significant for paleomagnetic studies of red beds.

5. Conclusions

In this study, a growth-CRM was imparted in 90 oriented cubic samples (2×2×2 cm^3) synthesized in different applied magnetic fields (< ~100 μT) to investigate the CRM acquisition and properties of the resulting magnetic minerals. The final synthetic magnetic products are a mixture of hematite and ferrihydrite or maghemite.

The CRM directions for these oriented samples closely follow that of the growth field when the field is above ~40 μT, however, CRM does not faithfully record the field direction once the field is lower than ~40 μT. The normalized intensity of CRM ($CRM/IRM_{@2.5T}$) is linearly related with the applied magnetic field according to theory prediction. Therefore, CRM recorded by hematite can in principle be used for relative paleointensity studies in earth-like field ranges, however, some cautions should be paid as CRM are poorly constrained in low fields.

The different blocking temperature spectrum can be used to discriminate CRM (gradual decay between ~200 and 650 °C) and DRM (most decay in the 600-680 °C range) in red beds. Further, thermal demagnetization curves of CRM have a concave shape while those of a DRM are convex in shape. This is a potential discriminator of CRM from DRM carried by hematite in natural media, and is significant for paleomagnetic studies of red beds.

Acknowledgments

Dr. Greig Paterson is thanked for meaningful discussion on the experiments. Han Peng and Su Kai are thanked for their help during CRM experiments. This study was supported by the National Natural Science Foundation of China (grants 41430962, 41374073, and 41025013). ZX Jiang further acknowledges support from the China Postdoctoral Science Foundation. LT acknowledges support from the NSF (EAR 1141840).

References

Bailey, M.E., Hale, C.J., 1981. Anomalous magnetic directions recorded by laboratory-induced chemical remanent magnetization. Nature 294, 739–741.

Barrón, V., Torrent, J., 2002. Evidence for a simple pathway to maghemite in Earth and Mars soils. Geochim. Cosmochim. Ac. 66, 2801–2806.

Barrón, V., Torrent, J., De Grave, E., 2003. Hydromaghemite, an intermediate in the hydrothermal transformation of 2-line ferrihydrite into hematite. Am. Mineral. 88, 1679–1688.

Bilardello, D., Kodama, K.P., 2010. Rock magnetic evidence for inclination shallowing in the early Carboniferous Deer Lake Group red beds of western Newfoundland, Geophys. J. Int. 181(1), 275-289.

Cogné, J., Halim, N., Chen, Y., Courtillot, V., 1999. Resolving the problem of shallow magnetizations of Tertiary age in Asia: insights from paleomagnetic data from the Qiangtang, Kunlun, and Qaidam blocks (Tibet, China), and a new hypothesis. J. Geophys. Res. 104, 17715–17734.

Collinson, D., 1965. The remanent magnetization and magnetic properties of red sediments. Geophys. J. R. Astron. Soc. 10, 105–126.

Collinson, D., 1966. Carrier of remanent magnetization in certain red sandstones. Nature 210, 516–517.

Collinson, D., 1974. The role of pigment and specularite in the remanent magnetism of red sandstones. Geophys. J. R. Astron. Soc. 38(2), 253–264.

Cox, A., 1969. Geomagnetic reversals. Science 163, 237–245.

Cox, A., 1975. The frequency of geomagnetic reversals and the symmetry of the nondipole field. Rev. Geophys. 13, 35–51.

Dekkers, M.J., 2012. End-member modelling as an aid to diagnose remagnetization: a brief review. Geological Society, London, Special Publications 371(1), 253–269.

Deng, C., Liu, Q., Wang, W., Liu, C., 2007. Chemical overprint on the natural remanent magnetization of a subtropical red soil sequence in the BoseBasin, southern China. Geophys. Res. Lett. 34, L22308, doi:22310.21029/22007GL031400.

Dunlop, D.J., Özdemir, Ö., 2001. Rock magnetism: fundamentals and frontiers, Cambridge University Press, Cambridge, United Kingdom.

Elmore, R.D., Dulin, S., Engel, M.H., Parnell, J., 2006. Remagnetization and fluid flow in the old red sandstone along the Great Glen Fault, Scotland. J. Geochem. Explor. 89, 96–99.

Gendler, T.S., Shcherbakov, V.P., Dekkers, M.J., Gapeev, A.K., Gribov, S.K., McClelland, E., 2005. The lepidocrocite–maghemite–haematite reaction chain—I. Acquisition of chemical remanent magnetization by maghemite, its magnetic properties and thermal stability. Geophys. J. Int. 160, 815–832.

Haigh, G., 1958. The process of magnetization by chemical change. Philos. Mag. 3, 267–286.

Hedley, I., 1968. Chemical remanent magnetization of the FeOOH, Fe_2O_3 system. Phys. Earth Planet. Int. 1, 103–121.

Huang, K., Opdyke, N.D., 1996. Severe remagnetization revealed from Triassic platform carbonates near Guiyang, Southwest China. Earth Planet. Sci. Lett. 143, 49–61.

Iosifidi, A.G., Mac Niocaill, C., Khramov, A.N., Dekkers, M.J., Popov, V.V., 2010. Palaeogeographic implications of differential inclination shallowing in permo-carboniferous sediments from the donets basin, Ukraine. Tectonophysics 490, 229–240.

Kent, D.V., Xu, G., Huang, K., Zhang, W., Opdyke, N.D., 1986. Paleomagnetism of upper Cretaceous rocks from South China. Earth Planet. Sci. Lett. 79(1), 179–184.

Kent, D.V., Zeng, X., Zhang, W.Y., Opdyke, N.D., 1987. Widespread late Mesozoic to Recent remagnetization of Paleozoic and lower Triassic sedimentary rocks from South China. Tectonophysics 139, 133–143.

Kruiver, P.P., Dekkers, M.J., Heslop, D., 2001, Quantification of magnetic coercivity components by the analysis of acquisition curves of isothermal remanent magnetization. Earth Planet. Sci. Lett.189, 269–276.

Kodama, K., Dekkers, M.J., 2004. Magnetic anisotropy as an aid to identifying CRM and DRM in red sedimentary rocks. Stu. Geophys. Geod. 48, 747–766.

Leonhardt, R., Fabian, K., 2007. Paleomagnetic reconstruction of the global geomagnetic field evolution during the Matuyama/Brunhes transition: Iterative Bayesian inversion and independent verification. Earth Planet. Sci. Lett. 253, 172–195.

Li, S., Deng, C., Yao, H., Huang, S., Liu, C., He, H., Pan, Y., Zhu, R., 2013.

Magnetostratigraphy of the Dali Basin in Yunnan and implications for late Neogene rotation of the southeast margin of the Tibetan Plateau. J. Geophys. Res. 118, 791–807.

Liu, C., Ge, K., Zhang, C., Liu, Q., Deng, C., Zhu, R., 2011. Nature of remagnetization of Lower Triassic red beds in southwestern China. Geophys. J. Int. 187, 1237–1249.

Liu, QS, Barron, V, Torrent, J, Eeckhout, S, Deng, CL, 2008. Magnetism of intermediate hydromaghemite in the transformation of 2-line ferrihydrite into hematite and its paleoenvironmental implications. J. Geophys. Res., 113, B01103, doi: 10.1029/2007JB005207.

Løvlie, R., Torsvik, T., Jelenska, M., Levandowski, M., 1984. Evidence for detrital remanent magnetization carried by hematite in Devonian red beds from Spitsbergen: palaeomagnetic implications. Geophys. J. Int. 79, 573–588.

Marshall, M., Cox, A., 1971. Effect of Oxidation on the Natural Remanent Magnetization of Titanomagnetite in Suboceanic Basalt. Nature 230, 28–31.

McCabe, C., Elmore, R.D., 1989. The occurrence and origin of Late Paleozoic remagnetization in the sedimentary rocks of North America. Rev. Geophys. 27, 471–494.

McClelland-Brown, E., 1982. Discrimination of TRM and CRM by blocking-temperature spectrum analysis. Phys. Earth Planet. Int. 30, 405–414.

McClelland, E., 1996. Theory of CRM acquired by grain growth, and its implications for TRM discrimination and palaeointensity determination in igneous rocks. Geophys. J. Int. 126, 271–280.

Michel, F.M., Barrón, V., Torrent, J., Morales, M.P., Serna, C.J., Boily, J.F., Liu, Q., Ambrosini, A., Cismasu, A.C., Brown, G.E., 2010. Ordered ferrimagnetic form of ferrihydrite reveals links among structure, composition, and magnetism. Proc. Nat. Acad. Sci. 107, 2787–2792.

Mitra, R., Tauxe, L., 2009. Full vector model for magnetization in sediments. Earth Planet. Sci. Lett. 286, 535–545.

O'Reilly, W., 1984. Rock and mineral magnetism, Blackie Son Limited, Bishopbriggs, Glasgow.

Özdemir, Ö., Dunlop, D.J., 1993. Chemical remanent magnetization during gamma-FeOOH phase transformations. J. Geophys. Res. 98, 4191–4198.

Robb, G.L., 1949. Red bed coloration. J. Sediment. Res. 19, 99–103.

Schwertmann, U., Cornell, R.M., 2000. Iron oxides in the laboratory, Wiley Online Library.

Stacey, F., Banerjee, S., 1974. The physical principles of rock magnetism, Elevier Sci. Publ. Comp., Amsterdam.

Stearns, C., Van der Voo, R., 1987. A paleomagnetic reinvestigation of the Upper Devonian Perry Formation: evidence for Late Paleozoic remagnetization. Earth Planet. Sci. Lett. 86, 27–38.

Steiner, M.B., 1983. Detrital remanent magnetization in hematite. J. Geophys. Res. 88, 6523–6539.

Stokking, L.B., Tauxe, L., 1987. Acquisition of chemical remanent magnetization by synthetic iron oxide. Nature 327, 610–612.

Stokking, L., Tauxe, L., 1990a. Properflies of chemical remanence in synthetic hematite: Testing theoretical predictions. J. Geophys. Res. 95, 12, 639–612,652.

Stokking, L.B., Tauxe, L., 1990b. Multicomponent magnetization in synthetic hematite. Phys. Earth Planet. Int. 65, 109–124.

Tan, X., Kodama, K.P., Chen, H., Fang, D., Sun, D., Li, Y., 2003. Paleomagnetism and magnetic anisotropy of Cretaceous red beds from the Tarim basin, northwest China: Evidence for a rock magnetic cause of anomalously shallow paleomagnetic inclinations from central Asia. J. Geophys. Res. 108(B2), 2107, doi:2110.1029/2001JB001608.

Tan, X., Kodama, K.P., Gilder, S., Courtillot, V., 2007. Rock magnetic evidence for inclination shallowing in the Passaic Formation red beds from the Newark basin and a systematic bias of the Late Triassic apparent polar wander path for North America. Earth Planet. Sci. Lett., 254(3–4), 345–357.

Tauxe, L., Kent, D.V., Opdyke, N.D., 1980. Magnetic components contributing to the NRM of Middle Siwalik red beds. Earth Planet. Sci. Lett. 47, 279–284.

Tauxe, L., Kent, D.V., 1984. Properties of a detrital remanence carried by haematite from study of modern river deposits and laboratory redeposition experiments. Geophys. J. R. Astron. Soc. 76, 543–561.

Tauxe, L., Kent, D.V., 2004. A simplified statistical model for the geomagnetic field and the detection of shallow bias in paleomagnetic inclinations: Was the ancient magnetic field dipolar? Timescales of the Paleomagnetic field, 101–115.

Tauxe, L., 2010. Essentials of paleomagnetism, University of California Press.

Tauxe, L., Gee, J., Steiner, M., Staudigel, H., 2013. Paleointensity results from the

Jurassic: New constraints from submarine basaltic glasses of ODP Site 801C. Geochem. Geophys. Geosyst. 14(10), 4718–4733.

Torrent, J., Schwertmann, U., 1987. Influence of hematite on the color of red beds. J. Sediment. Res. 57, 682–686.

Valet, J.P., Meynadier, L., Guyodo, Y., 2005. Geomagnetic dipole strength and reversal rate over the past two million years. Nature 435, 802–805.

Van der Voo, R., Torsvik, T.H., 2012. The history of remagnetization of sedimentary rocks: deceptions, developments and discoveries. Geological Society, London, Special Publications 371(1), 23–53.

Van Houten, F.B., 1968. Iron oxides in red beds. Geol. Soc. Am. Bull. 79, 399–416.

Van Houten, F.B., 1973. Origin of red beds: a review-1961-1972. Annual Rev. Earth Planet. Sci. 1, 39–61.

Walker, T.R., 1967. Color of recent sediments in tropical Mexico: a contribution to the origin of red beds. Bull. Geol. Soc. Am. 78, 917–920.

Wang, Z., Van der Voo, R., 1993. Pervasive remagnetization of Paleozoic rocks acquired at the time of Mesozoic folding in the South China Block. J. Geophys. Res. 98, 1729–1741.

Yan, M., Van der Voo, R., Fang, X.M., Parés, J.M., Rea, D.K., 2006. Paleomagnetic evidence for a mid-Miocene clockwise rotation of about 25° of the Guide Basin area in NE Tibet. Earth Planet. Sci. Lett. 241, 234–247.

Table 1. Summary of the field conditions in the chemical remanent magnetization experiments. CRM is the remanence measured after the growth experiment and ChRM the remanence measured after thermal demagnetization between 200 and 640°C.

	Applied field			CRM			ChRM		
sample series	declination	inclination	intensity(μT)	declination	inclination	error (ΔD/ΔI)	declination	inclination	error (ΔD/ΔI)
CRM1	5.9	-42.2	100.8	1.6	-35.5	-4.3/6.7	-0.5	-29.5	-6.4/12.7
CRM2	4.5	-48.5	85.7				No thermal demagnetization		
CRM3	9.4	-53.7	67.6	6.6	-40.3	-2.8/13.4	2.9	-38.5	6.5/15.2
CRM4	3	48.9	54.7				No thermal demagnetization		
CRM5	2.7	36.2	44.2	8.3	36.8	-5.6/0.6	No thermal demagnetization		
CRM6	-15.4	-41.2	37.9	1.9	-28.3	17.3/12.9	2.2	-34.7	17.6/6.5
CRM7	-3.4	33.8	24.2	11.1	47	14.5/13.2	No thermal demagnetization		
CRM8	-26.5	-38.1	16.2	27.3	-78.6	53.8/40.5	43.7	-79.7	70.2/41.6
CRM9	-10	51.4	11.9	40.7	65	50.7/13.6	No thermal demagnetization		

Table 2. IRM component analysis of representative CRM samples (cf. Kruiver et al., 2001). $B_{1/2L}$ and $B_{1/2H}$ are the $B_{1/2}$ (mT) (the medium field at which half of the IRM is reached) of low and high coercivity component, DP is the dispersion parameter of each IRM component. The IRM contribution (%) is the contribution of each IRM component to the total IRM.

sample name	component L			component H		
	$B_{1/2L}$ (mT)	DP	IRM contribution(%)	$B_{1/2H}$ (mT)	DP	IRM contribution(%)
CRM1	40	0.26	5	1995	0.40	95
CRM3	32	0.2	2	1778	0.45	98
CRM6	22	0.25	15	891	0.55	85
CRM8	40	0.30	9	891	0.40	91

Table 3. Summary of reference data used in Figure 8.

Reference	locality	mineralogy	age	remanent type
Tauxe et al. (1980)	Middle Siwalik	Hematite pigment, specular hematite	Miocene	CRM & DRM
Kent et al. (1987)	Yichang, China	hematic sandstone	upper Devonian	CRM
Stokking & Tauxe (1987)	growth in the lab	hematite pigment		CRM
Cogné et al.(1999)	Qiangtang block of Tibet	red sandstone	Eocene	DRM
Løvlie et al.(1984)	North Central Spitsbergen	sandstone composed of hematite granules	Devonian	DRM
Yan et al.(2006)	Gonghe-GuideBasin	mudstones and siltstones	Miocene	DRM
Liu et al.(2011)	Yunnan province	Limestones interbedded with mudstones and sandstones	uppermost Permian	CRM

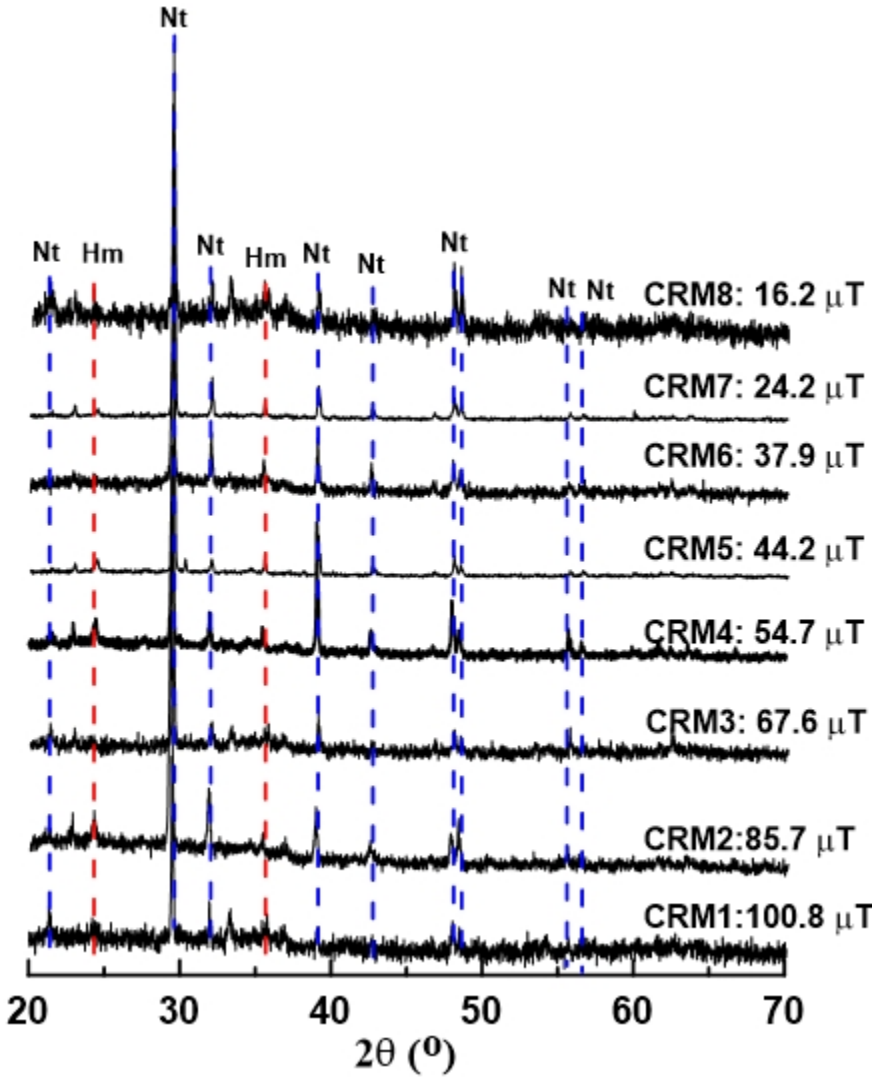

Figure 1. X-ray diffractograms of samples grown in different applied magnetic fields. The red and blue lines represent the characteristic reflections of hematite and sodium nitrate ($NaNO_3$), respectively, where Hm and Nt are the abbreviations of hematite and sodium nitrate.

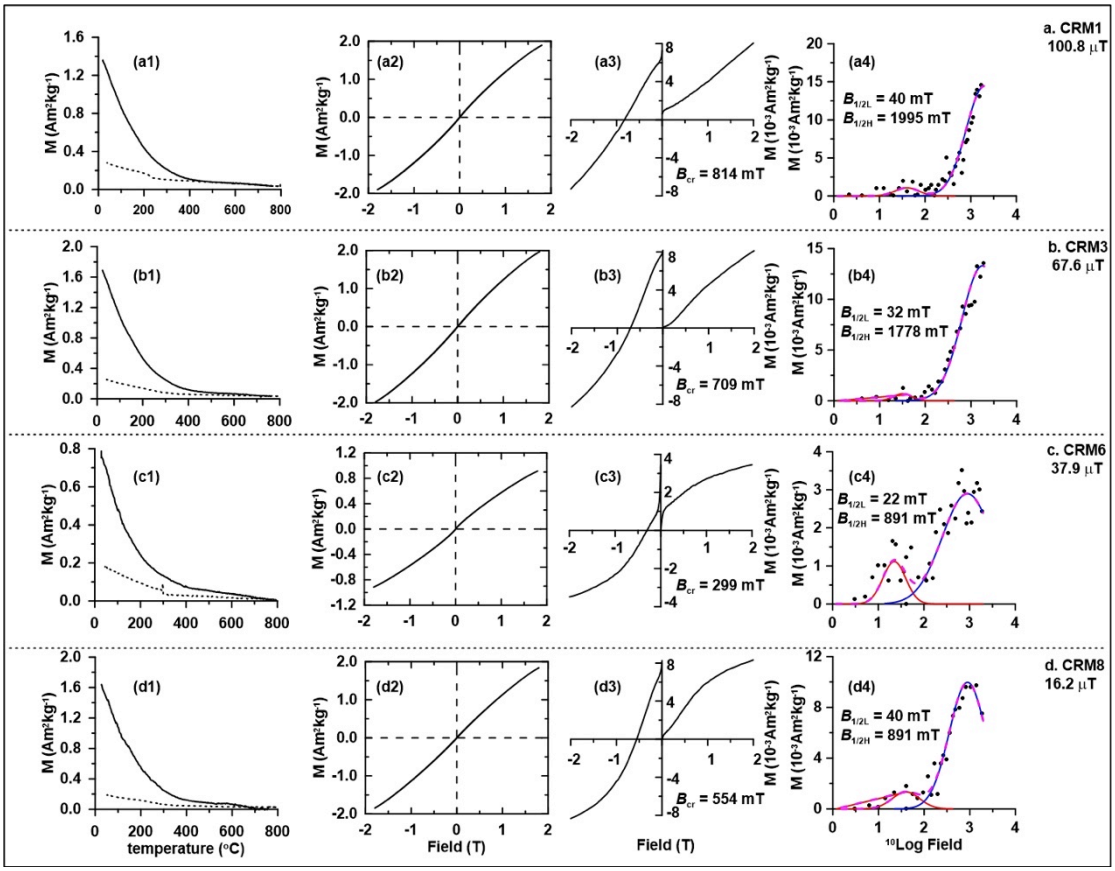

Figure 2. The rock magnetic properties of some representative samples. (a1, b1, c1, d1) Thermomagnetic curves (J-T) in air, where the solid and dashed lines are the heating and cooling branches; (a2, b2, c2, d2) Hysteresis loops; (a3, b3, c3, d3) Acquisition curves of isothermal ramanent magnetization (IRM) and back-field demagnetization curves; (a4, b4, c4, d4) IRM component analysis, where the red, blue, and purple lines indicate the low coercivity, high coercivity components and the sum of these components. The solid points represent the raw IRM gradient data.

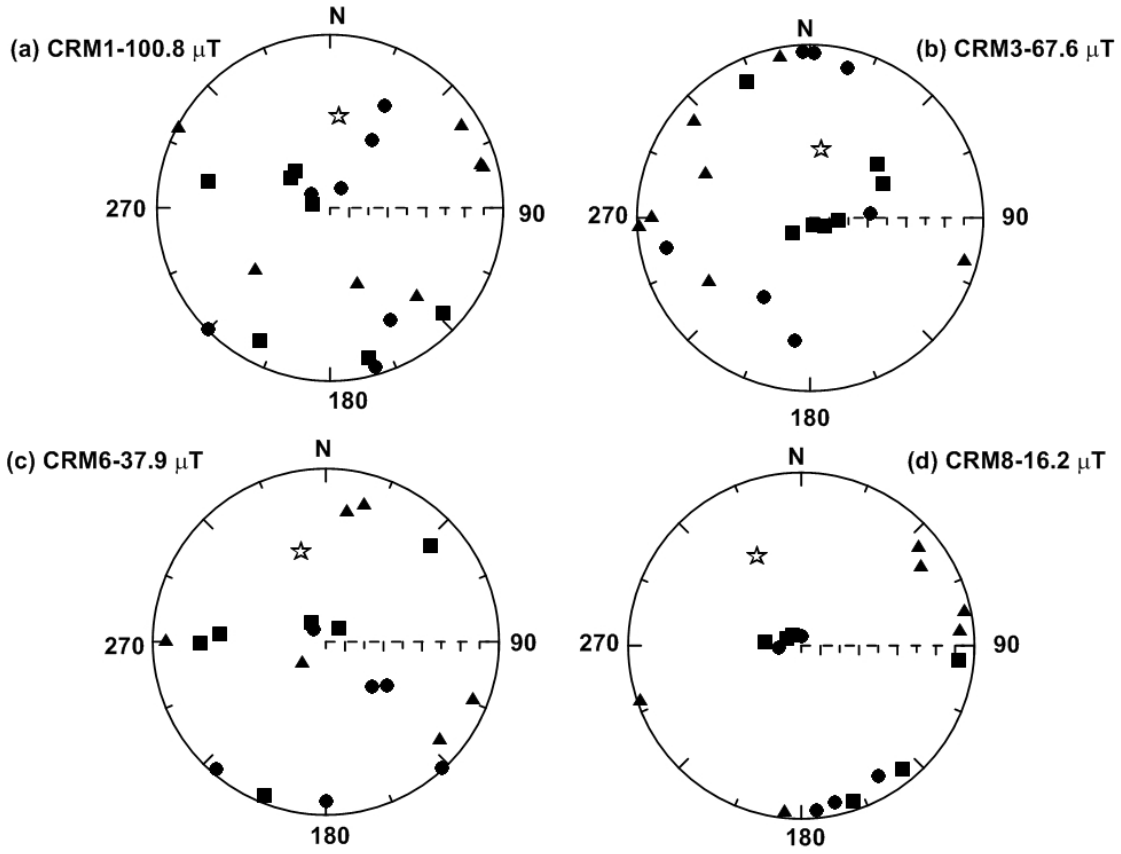

Figure 3. The anisotropy of magnetic susceptibility (AMS) of samples grown in different applied magnetic fields, where the squares, triangles, and circles represent the maximum magnetic susceptibility (K_{max}), the intermediate magnetic susceptibility(K_{int}), and the minimum magnetic susceptibility (K_{min}) axes, respectively. The stars indicate the direction of the applied magnetic field during CRM acquisition.

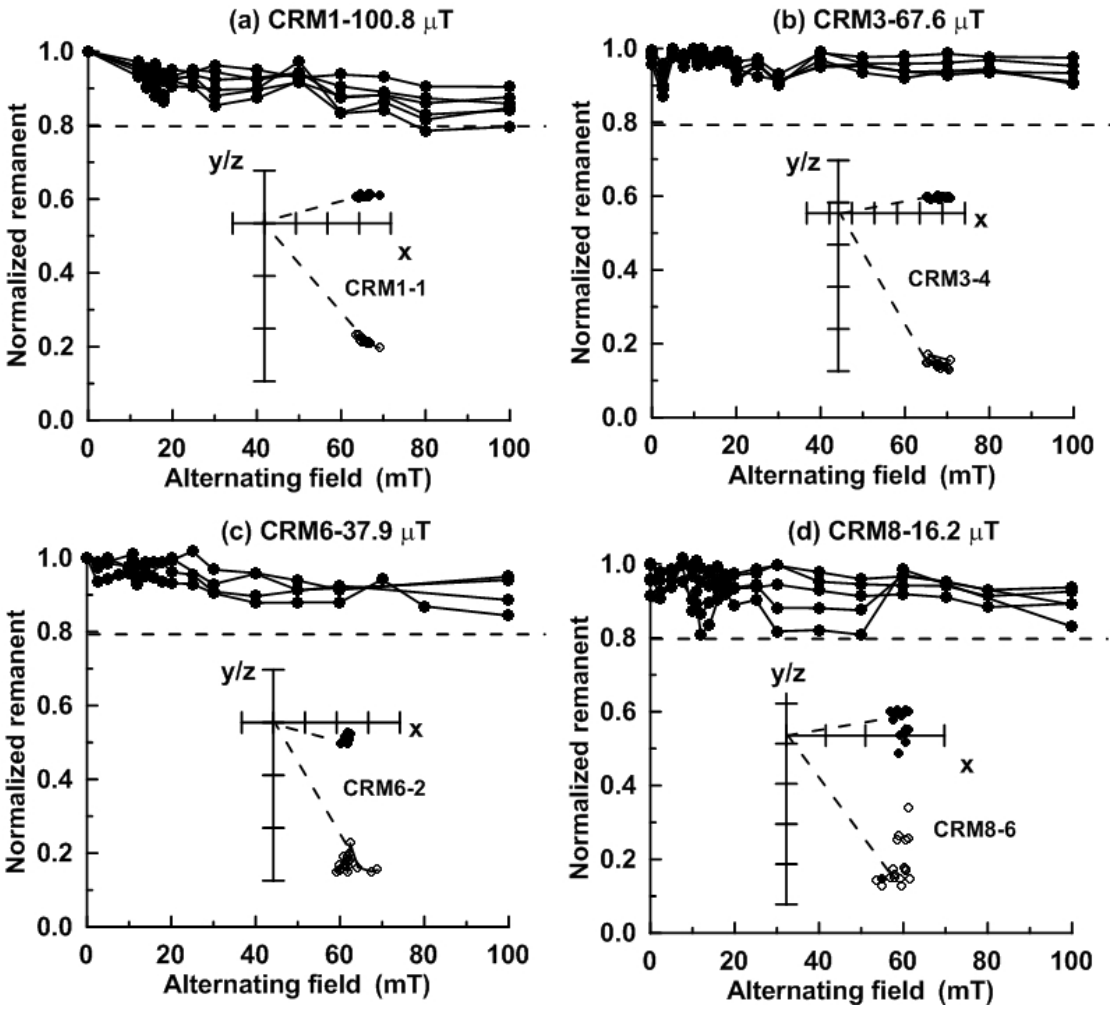

Figure 4. Alternating field (AF) demagnetization curves of chemical remanent magnetization (CRM) for the series of samples: (a) CRM1-100.8 μT, (b) CRM6-67.6μT, (c) CRM6-37.9μT and (d) CRM8-16.2 μT. The insets show the orthogonal projections of progressive AF demagnetization for representative samples. The solid and open circles represent the horizontal and vertical projections, respectively.

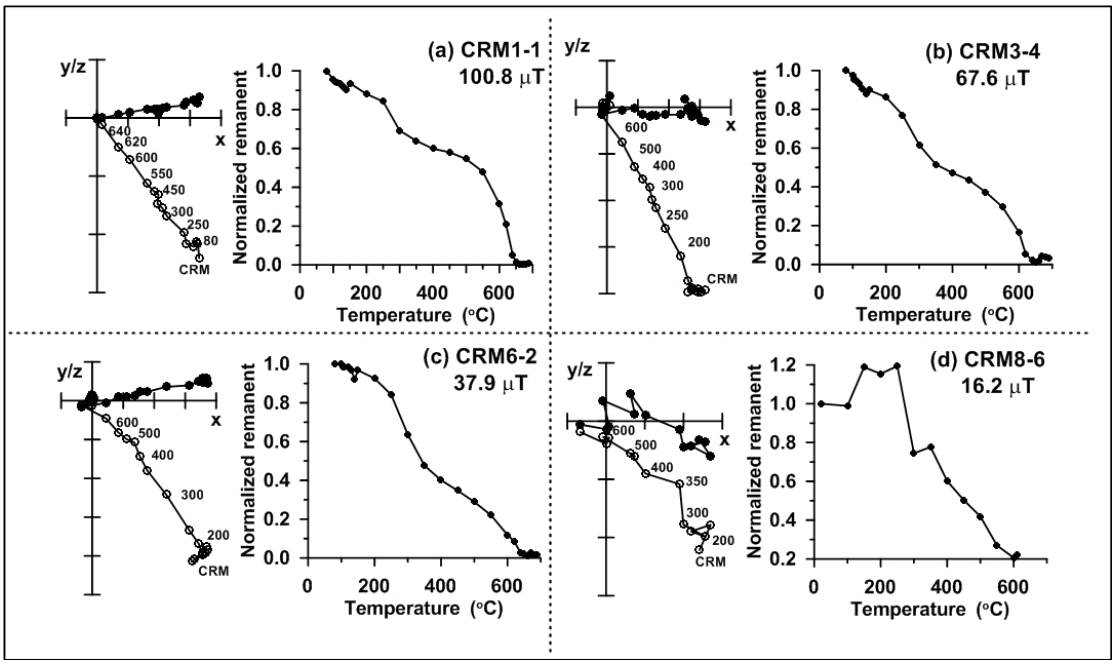

Figure 5. Representative orthogonal projections of stepwise thermal demagnetization of chemical remanent magnetization (CRM) after AF demagnetization. (a) CRM1-1; (b) CRM3-4; (c) CRM6-2; and (d) CRM8-6. In the left-handed panels, the solid and open circles represent the horizontal and vertical projections, respectively. The decay curves normalized to the starting CRM intensity after the AF demagnetization are shown in the right-handed panels.

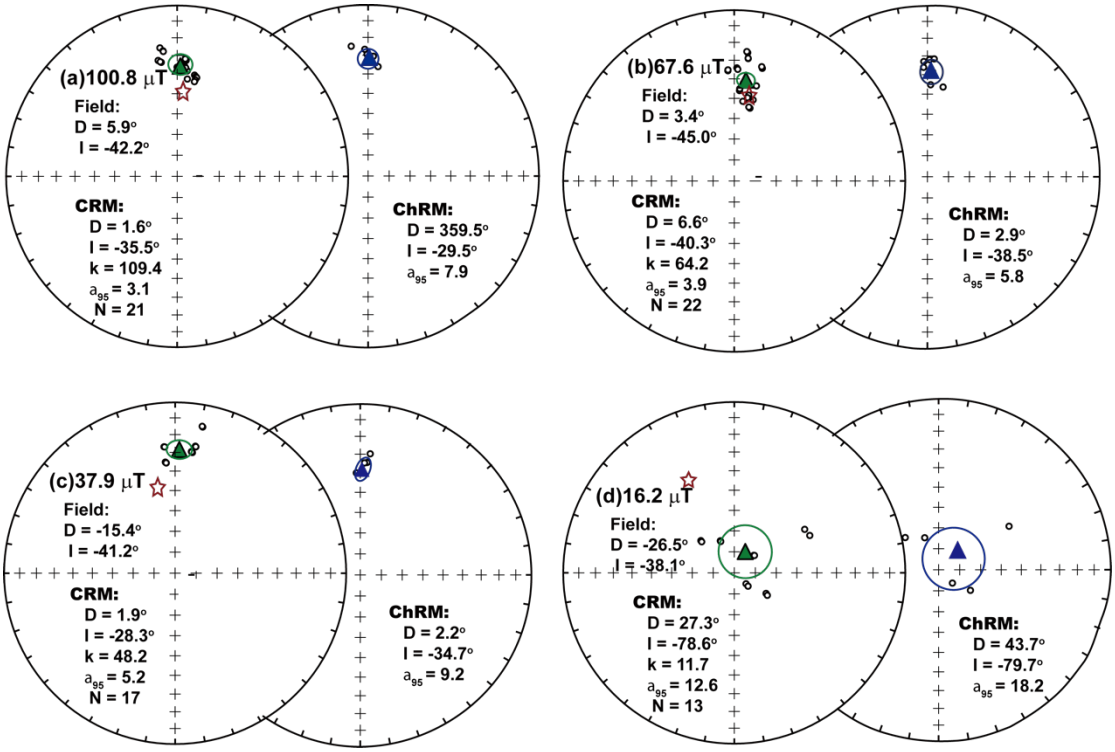

Figure 6. Equal area projections of the directions of the starting chemical remanent magnetization (CRM), applied magnetic field (red star), and characteristic remanent magnetization (ChRM) retrieved after stepwise thermal demagnetization. The green and blue triangles show the mean directions of CRM and ChRM, ellipsoids represent the 95% confidence limits.

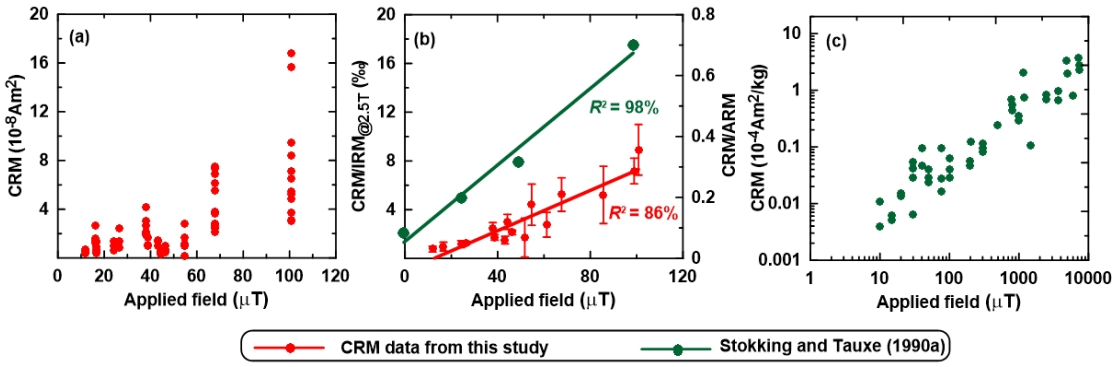

Figure 7. Diagrams of chemical remanent magnetization (CRM) intensity versus applied field. (a) the original data of CRM intensity versus applied field for our data set; (b) $CRM/IRM_{@2.5T}$ (red: our data, $IRM_{@2.5T}$, isothermal remanent magnetization acquired at 2.5 T field) or CRM/ARM (green; data from Stokking and Tauxe (1990a)) versus applied field; (c) CRM data from Stokking and Tauxe (1990a) versus applied field (10 – 7500 μT).

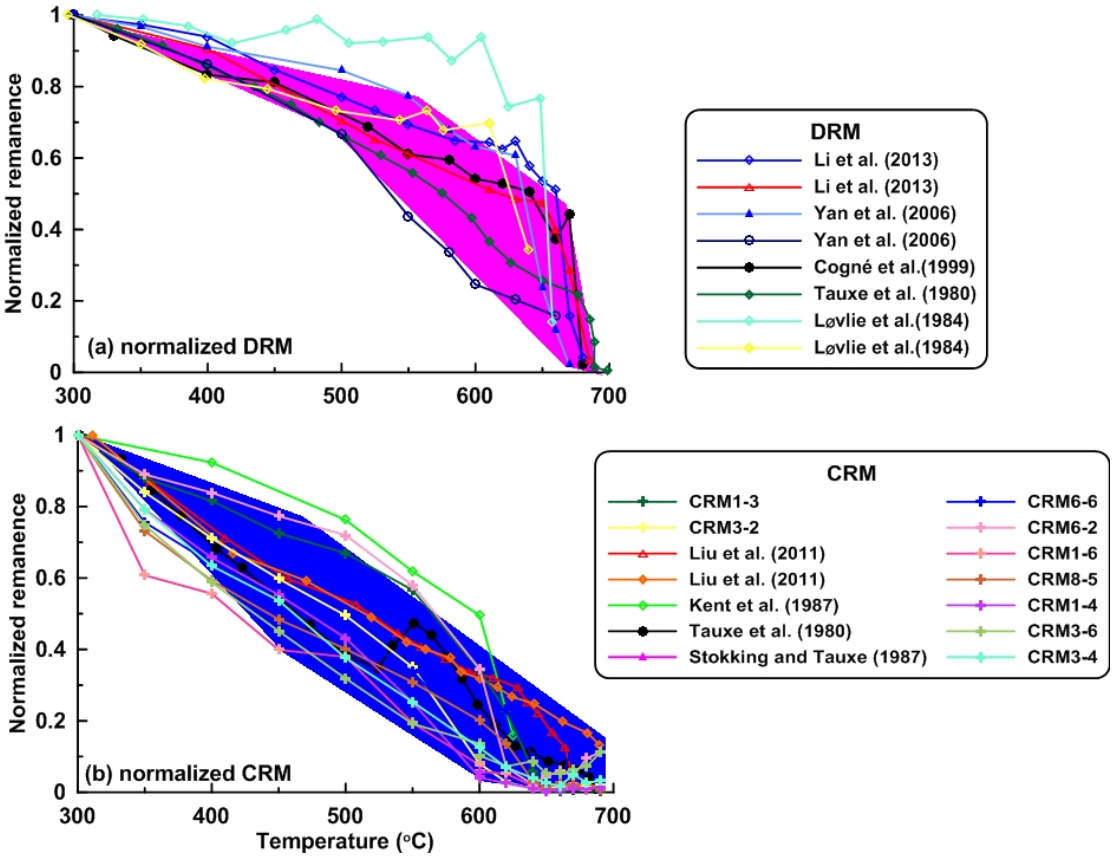

Figure 8. Stepwise thermal demagnetization curves of (a) detrital remanent magnetization (DRM) and (b) chemical remanent magnetization (CRM) for our samples and some reference data. Data were normalized at the 300 °C step to remove the influence of potentially present viscous remanent magnetization.